

# Analysis of depth-of-focus of synthetic aperture antenna arrays

Bertrand M. Lucotte\* and Andrew R. Harvey

School of Engineering and Physical Sciences, Heriot-Watt University, Edinburgh EH14 4AS, UK

\*Corresponding author: bl13@hw.ac.uk

Received March 4, 2010; revised May 17, 2010; accepted May 18, 2010;  
posted May 28, 2010 (Doc. ID 125015); published June 9, 2010

Interferometric synthetic aperture arrays (SAA) can be refocused at any range via digital processing of the raw data, called the visibility function. Such systems are sensitive, however, to ranging errors in digital refocusing. They, therefore, exhibit a limited depth of focus, because these errors are equivalent to introducing defocus in the system. We derive an analytical expression for the Strehl ratio of synthetic aperture arrays, which accounts for both the antenna voltage pattern and the focal shift factor encountered in imaging systems with a low Fresnel number. Assessment of the depth of focus of short-range imaging arrays is allowed and is illustrated for common array designs. © 2010 Optical Society of America

OCIS codes: 280.6730, 120.5800, 040.1240, 110.6795, 110.3175.

In interferometric synthetic aperture radiometers, the image is formed digitally after sampling of the visibility function by the antenna array [1–3]. Because of the coherent detection, digital refocusing can then be performed by adequate adjustment of phase terms in the digital image reconstruction. This is similar, in principle, to the interferometric synthetic aperture microscopy technique [4]. For the high spatial resolution of synthetic aperture arrays (SAA) to be maintained throughout a 3D volume, it is necessary to digitally focus on each point on the surfaces being imaged, and the depth of field (DoF) of the SAA determines the accuracy with which this must be accomplished and also the blurring characteristics of out-of-focus planes. We show here, using a Strehl ratio metric, that the DoF characteristics vary significantly with the SAA parameters and also that they are significantly different from those for an equivalent conventional imager. Range focusing errors in SAA are mathematically equivalent to defocus in a conventional optical system. The DoF of a conventional optical system can be defined in terms of its Strehl ratio, as was first proposed by Rayleigh [5]. We apply here this approach to obtain the first characterization of the DoF of interferometric SAA.

The defocus parameter  $W_{20}$  quantifies the severity of the defocus effect. It is expressed here in units of wavelengths and defined in object space because the image is formed digitally in SAA:

$$W_{20} = \frac{a^2 z}{2\lambda f(f+z)}, \quad (1)$$

with  $a$  being the radius of the aperture of the array,  $\lambda$  the center wavelength of the receivers,  $f$  the focusing range, i.e., the focal length introduced in the digital image formation, and  $z$  the axial displacement of the target from the focal plane oriented positively away from the array. To describe the pupil function of the array, we first define the pupil function  $P_0(\rho'/a) = P_0(\rho)$  of a circular aperture system (with radius  $a$ ) in the presence of defocus, with  $\rho'$  and  $\rho$  the absolute and normalized radial pupil variables, respectively:

$$P_0(\rho) = p(\rho) \exp[j2\pi W_{20}\rho^2], \quad (2)$$

$$p(\rho) = \begin{cases} 1 & |\rho| \leq 1, \\ 0 & |\rho| > 1, \end{cases} \quad (3)$$

We define the parameter  $\rho_a = b/a$ , where  $b$  is the radius of the aperture of a single antenna. The defocused pupil function of the array  $P(\rho, W_{20})$  is obtained from Eq. (2) after modification of the amplitude pupil function:

$$P(\rho, W_{20}) = e^{j2\pi W_{20}\rho^2} \sum_{k=1}^{k=N} \delta(\rho - \rho_k) ** p\left(\frac{\rho}{\rho_a}\right), \quad (4)$$

where  $**$  denotes the two-dimensional convolution product,  $\rho = (x, y)$  is the pupil-plane Cartesian vector coordinate, and  $\rho_k$  is the vector coordinate of the center of antenna  $k$ . When  $f \gg a \gg \lambda$ , the impulse response  $\hat{P}(\mathbf{r}, W_{20})$  of the array is proportional to the Fourier transform of the pupil function  $P(\rho, W_{20})$  within the paraxial approximation [5]:

$$\hat{P}(\mathbf{r}, W_{20}) = \frac{-j e^{jkz} a^2}{\lambda f(f+z)} \int_{-1}^{+1} \int_{-1}^{+1} P(\rho, W_{20}) \times \exp\left[-j \frac{2\pi a}{\lambda f} (\xi x + \eta y)\right] d\xi d\eta, \quad (5)$$

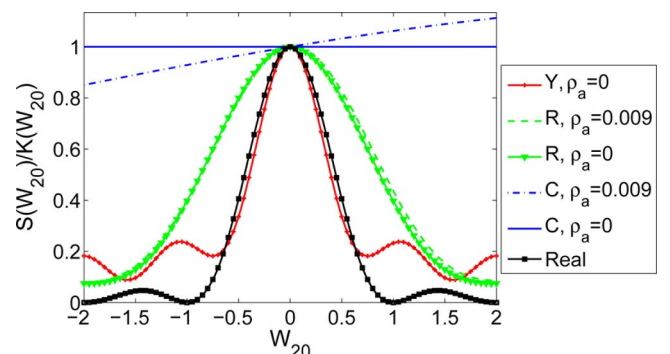


Fig. 1. (Color online)  $S(W_{20})/K(W_{20})$  for the power-law  $Y$  array (Y), Reuleux triangle array (R), circular array (C), and real circular aperture system (Real).  $\rho_a \sim 0.0091$  and  $N_F = 20$ .

where  $\mathbf{r} = (x, y)$  denotes the object-plane Cartesian vector coordinate. Using the change of coordinates  $u = ax/\lambda f$ ,  $v = ay/\lambda f$  and ignoring the unimportant phase factor  $kz$  in Eq. (5),  $\hat{P}(\mathbf{r}, W_{20})$  is reduced to

$$\hat{P}(\mathbf{r}, W_{20}) = \frac{N_F - 2W_{20}}{f} \sum_{k=1}^{k=N} p\left(\frac{\rho_k}{\rho_a}\right) \exp[j2\pi(W_{20}\rho_k^2 + u\xi_k + v\eta_k)], \quad (6)$$

$$= \frac{N_F - 2W_{20}}{f} \sum_{k=1}^{k=N} F_k(\mathbf{r}, W_{20}) \exp[j2\pi(W_{20}\rho_k^2 + u\xi_k + v\eta_k)], \quad (7)$$

where  $N_F = a^2/\lambda f$  is the Fresnel number of the array aperture, and

$$F_k(\mathbf{r}, W_{20}) = V_k(\mathbf{r}, W_{20}) \iint p\left(\frac{\rho}{\rho_a}\right) \exp(j2\pi W_{20}\rho^2) \exp[-j2\pi(\xi\alpha + \eta\beta)] d\xi d\eta, \quad (8)$$

where  $\xi$  and  $\eta$  are dummy variables representing the normalized pupil coordinates,  $\alpha = u + 2W_{20}\xi_k$ ,  $\beta = v + 2W_{20}\eta_k$ , and  $V_k(\mathbf{r}, W_{20})$  is a unity factor introduced here for later convenience. The variables  $\alpha$  and  $\beta$  describe the lateral displacement of the diffracted field contribution from each subaperture that is associated with the focus error. Equation (8) is a Fresnel transform and can also be viewed as the Fourier transform of a rotationally symmetric function. Thus  $F_k(\mathbf{r}, W_{20})$  depends on the radial variable  $\zeta = (\alpha^2 + \beta^2)^{1/2}$ :

$$F_k(\mathbf{r}, W_{20}) = 2\pi V_k(\mathbf{r}, W_{20}) \int_0^{\rho_a} \exp(j2\pi W_{20}\rho^2) \times J_0(2\pi\zeta\rho) \rho d\rho, \quad (9)$$

where  $J_0(x)$  is the Bessel function of the first kind of order zero.  $F_k(0, 0)$  is equal to the normalized area of the antenna dish  $\pi\rho_a^2$ . Equations (7) and (9) describe the impulse response of an optical system with the generalized pupil function given in Eq. (4). The impulse response of SAA is determined by both the array pattern and voltage pattern  $V_k(\mathbf{r}, W_{20})$  of each antenna, which is written for circular antennas as

$$V_k(\mathbf{r}, W_{20}) \propto \frac{J_1[2\pi b\gamma(N_F - 2W_{20})/a^2]}{2\pi b\gamma(N_F - 2W_{20})/a^2}, \quad (10)$$

where  $\gamma = [(x - a\xi_k)^2 + (y - a\eta_k)^2]^{1/2}$ . For simplicity  $F_k(\mathbf{r}, W_{20})$  will be expressed as

$$F_k(\mathbf{r}, W_{20}) = A_k \exp(j\theta_k). \quad (11)$$

The point-spread function (PSF) of the array,  $h(\mathbf{r}, W_{20})$ , is equal to the square modulus of the coherent impulse response. Combining Eqs. (7) and (11), one can express the on-axis value of the defocused PSF as

$$h(0, W_{20}) = 2 \frac{(N_F - 2W_{20})^2}{f^2} \sum_{m=1}^{m=N} \sum_{n=m+1}^{n=N} A_m A_n \times \cos[2\pi W_{20}(\rho_m^2 - \rho_n^2) + \theta_m - \theta_n]. \quad (12)$$

Note that the autocorrelation terms in Eq. (12), i.e., terms for which  $m = n$ , are excluded from the sum because they do not participate in the image formation of interferometric SAA. Similarly to the definition used in [6] the Strehl ratio  $S(W_{20})$  is defined here as

$$S(W_{20}) = \frac{h(0, W_{20})}{h(0, 0)} = \frac{|\hat{P}(0, W_{20})|^2}{|\hat{P}(0, 0)|^2}. \quad (13)$$

Combining Eqs. (12) and (13) the Strehl ratio of an SAA is

$$S(W_{20}) = \frac{K(W_{20})}{(\pi\rho_a^2)^2 B} \sum_{m=1}^{m=N} \sum_{n=m+1}^{n=N} A_m A_n \times \cos[2\pi W_{20}(\rho_m^2 - \rho_n^2) + \theta_m - \theta_n], \quad (14)$$

$$K(W_{20}) = \frac{(N_F - 2W_{20})^2}{N_F^2}, \quad (15)$$

where  $B = \sum_{m=1}^{m=N} \sum_{n=m+1}^{n=N} V_m(0, 0) V_n(0, 0)$ . Equation (14) constitutes the main result of this letter and can be used to characterize the DoF of interferometric SAA. Three special cases are now considered. First, the Strehl ratio  $S_{\text{real}}(W_{20})$  of a circular real aperture optical system is obtained by combination of Eqs. (7), (9), and (13):

$$S_{\text{real}}(W_{20}) = K(W_{20}) \text{sinc}^2(W_{20}), \quad (16)$$

with  $\text{sinc}(x) = \sin(\pi x)/(\pi x)$ . This is in agreement with the expression derived in [6]. The factor  $K(W_{20})$  in Eqs. (14) and (16) and detailed in Eq. (15) is constant and equal to unity for Fresnel numbers that are large compared to unity, typically  $N_F \geq 100$ . It can therefore be neglected in most systems operating at visible wavelengths. However, this factor becomes significant when  $N_F < 100$  and is then responsible for the axial shift of the maximum axial intensity away from the focal plane and toward the exit pupil. This effect, previously described in [6–8], occurs in millimeter-wave short-range imaging, e.g., a personnel scanner, where typically  $N_F \sim 20$  for  $f = 2$  m,  $a = 35$  cm, and  $\lambda = 3$  mm. The Strehl ratio  $S_0(W_{20})$  in the limit case  $b = 0$  is readily obtained from Eq. (6) and (13):

$$S_0(W_{20}) = \frac{2K(W_{20})}{N(N-1)} \sum_{m=1}^{m=N} \sum_{n=m+1}^{n=N} \cos[2\pi W_{20}(\rho_m^2 - \rho_n^2)]. \quad (17)$$

Because  $K(W_{20})$  is independent of the array configuration, it is clear from Eq. (17) that an array of antennas distributed on a circle maximizes  $S_0(W_{20})$ . If one

accounts for the finite radius of the antennas, the Strehl ratio  $S_{\text{cir}}(W_{20})$  for a circular array is readily obtained from Eq. (14):

$$S_{\text{cir}}(W_{20}) = \frac{2K(W_{20})}{N(N-1)V_0(0,0)} \frac{1}{(\pi\rho_a^2)^2} \sum_{m=1}^{m=N} \sum_{n=m+1}^{n=N} A_m A_n \times \cos(\theta_m - \theta_n). \quad (18)$$

Equations (14), (18), and (18) are useful in the design of short-range imaging antenna arrays with a specific DoF. To illustrate this, the Strehl ratio of three 27-antenna arrays are calculated: (i) a conventional power-law Y-shaped array [1,9], denoted  $Y$ , with a power parameter of 1.7, (ii) a Reuleux triangle array, denoted  $R$ , and (iii) a circular array, denoted  $C$ . Note that similar to  $C$  arrays, the  $R$  array samples the Fourier domain with an isotropic cutoff frequency [10,11]. These results are compared with the Strehl ratio of a real circular aperture system, denoted  $\text{Real}$ . The ratio  $S(W_{20})/K(W_{20})$ , shown in Fig. 1 for  $N_F = 20$ , solely depends on the array geometry and therefore fully characterizes the effect of the array configuration on the DoF of the array. The effect on  $S(W_{20})/K(W_{20})$  of the term  $F_k(0, W_{20})$  due to finite-size antennas is presented for the  $R$  and  $C$  arrays, with  $\rho_a \sim 0.0091$ , corresponding to an antenna radius  $b = \lambda$  for the  $C$  array ( $\lambda = 3.2$  mm). The parameter  $W_{20}$  was recalculated to account for the change in aperture due to finite-size antennas. The increase in  $S(W_{20})/K(W_{20})$  with the antenna size  $\rho_a$  observed for  $W_{20} > 0$  is primarily due to the antenna voltage pattern. For antenna elements such that  $b \leq \lambda/2$  ( $\rho_a \sim 0.005$ ), as typically employed in mm-wave SAA,  $S_0(W_{20})$  provides a good approximation to  $S(W_{20})$  over the range  $|W_{20}| \leq 2$ . The error of this approximation decreases with lower values of  $N_F$  and is 1.2% and 1.9% for the  $R$  and  $C$  arrays, respectively at  $\rho_a \sim 0.005$  and  $N_F = 20$ . The variation in  $S(W_{20})$  with  $N_F$  is shown in Fig. 2 for (a)  $N_F = 20$  and (b)  $N_F = 5$ . It is assumed that only  $f$  is varied and that the other parameters remain unchanged. The DoF limits of SAA are determined according to the threshold  $S(W_{20}) \geq 0.8$ . The  $R$  and  $C$  arrays are shown to achieve increased DoF compared to the real aperture system, with DoF limits  $W_{20} = [-0.6, 0.4]$  and  $W_{20} = [-37, 1.1]$ , respectively, compared to  $W_{20} = [-0.25, 0.2]$  for the real aperture system with  $N_F = 20$ . For  $N_F = 5$ , these limits become  $W_{20} = [-0.95, 0.2]$ ,  $W_{20} = [-52.9, 0.25]$ , and  $W_{20} = [-0.35, 0.15]$  for the  $R$  array,  $C$  array, and the real aperture system, respectively ( $\rho_a = 0.005$ ). In summary, an analytical expression for the Strehl ratio of SAA was derived and accounts for the directive voltage pattern of finite-sized antennas and the focal shift factor encountered in imaging systems with a low Fresnel number. This expression allows immediate

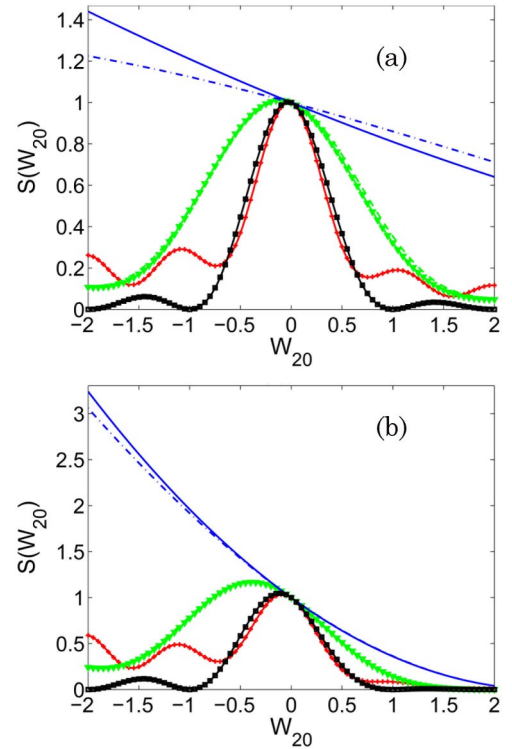


Fig. 2. (Color online)  $S(W_{20})$  for the same systems as in Fig. 1 (with the same legend). (a)  $N_F = 20$  and (b)  $N_F = 5$ .

assessment of the DoF of short-range imaging interferometric arrays and may be used in the design of such systems.

This work has been funded by QinetiQ.

## References

1. A. R. Thompson, J. M. Moran, and G. W. Swenson, *Interferometry and Synthesis in Radio Astronomy* (Wiley, 2001).
2. F. Torres, A. Camps, J. Bará, and I. Corbella, *Radio Sci.* **32**, 629 (1997).
3. A. R. Harvey and R. Appleby, *Aeronaut J.* **107**, 87 (2003).
4. B. J. Davis, T. S. Ralston, D. L. Marks, S. A. Boppart, and P. S. Carney, in *Proceedings of the IEEE International Conference on Image Processing 2007* (IEEE, 2007), Vol. IV, pp. 145–148.
5. M. Born and E. Wolf, *Principles of Optics* (Cambridge U. Press, 1999).
6. J. Ojeda-Castañeda, M. Martínez-Corral, P. Andrés, and A. Pons, *Appl. Opt.* **33**, 7611 (1994).
7. Y. Li and E. Wolf, *Opt. Commun.* **39**, 211 (1981).
8. Y. Li and E. Wolf, *J. Opt. Soc. Am. A* **1**, 801 (1984).
9. Y. L. Chow, *IEEE Trans. Antenn. Propag.* **20**, 30 (1972).
10. E. Keto, *Astrophys. J.* **475**, 843 (1997).
11. B. M. Lucotte, B. Grafulla-González, and A. R. Harvey, *Radio Sci.* **44**, RS1006 (2009).